Nuclear Engineering and Design 424 (2024) 113312

Contents lists available at ScienceDirect

Nuclear Engineering and Design

journal homepage: www.elsevier.com/locate/nucengdes

Investigation of jet induced by direct contact condensation using PIV

M. Pellegrini [a,*], K. Okamoto [a], B. Blaisot [b], N. Erkan [c]

[a] Nuclear Professional School, Graduate School of Engineering, The University of Tokyo, 7-3-1 Hongo, Bunkyo-ku, 113-8656, Japan
[b] Institut de Mécanique des Fluides de Toulouse, Université de Toulouse (INPT, UPS) and CNRS, Allée C. Soula, 31400 Toulouse, France
[c] Fusion Technology Facility, United Kingdom Atomic Energy Authority (UKAEA), Advanced Manufacturing Park, Rotherham S60 5FX, UK

ARTICLE INFO

Keywords:
Direct Contact Condensation
PIV
Chugging
Jet
Bubbling
Entrainment

ABSTRACT

Steam Direct Contact Condensation (DCC) is an effective way to condense steam in a pool of water. This method of condensation is widely employed in the containment of nuclear power plants. One of the limitations of DCC is the generation of non-uniform temperature distribution in the water pool, which can result in slow but steady pressurization of the containment. Due to the non-linearity of the problem the evaluation of the temperature distribution in the pool cannot be established by simple theoretical analyses but computational models are deemed necessary (e.g. Computational Fluid Dynamics (CFD) and Lumped Parameter (LP) codes). Existing models could be validated only qualitatively because the experimental evidence is composed fundamentally of video acquisitions, which does not allow for a correct comparison of the phenomena. In this paper the authors will present PIV results of a small-scale facility during DCC measuring the jet induced by chugging. The authors have found that the water flow induced by the bubble implosion contains several similarities with continuous and synthetic jets (e.g. velocity spreading) following the self-similar properties of the jet theory. The period of the implosion can be quantified with the current methodology to be around 0.025 s and it has been shown to be independent on the water temperature.

1. Introduction

Steam Direct Contact Condensation (DCC) is an effective way to condense steam in a pool of water. Its application is of particular importance in Nuclear Power Plants (NPP) with reduced containment size (e.g. BWR) where DCC is primarily employed to suppress harmful pressure surges, resulting from direct release of steam during an accident. In general, gas can be discharged from large pipes (i.e. vent pipes) during a Loss of Coolant Accident where two phases of gas discharge can be observed (Lahey and Moody, 0000). The first includes a mixture of steam and non-condensable gases, followed by pure steam injection. In addition pure saturated steam is transferred to the Suppression Chamber (S/C) from multi-holes T-quenchers connected to the Safety Relief Valves. Finally saturated steam can be discharged from the quenchers connected to the outlet of turbo-pumps such as the Reactor Core Isolation Cooling system or the High Pressure Coolant Injection system (Pellegrini et al., 2016) The same technology is also expanded to wet-scrubbers to remove harmful contaminants in nuclear power plants (Pellegrini et al., 2016; NEA/CSNI/R, 2009) in the postulated case of an accident, and few applications were extended more recently to diesel engines (Abdulwahid et al., 2018).

One of the limitations of DCC is the generation of non-uniform temperature distribution in the water pool which can result in slow but steady pressurization of the containment. The occurrence of such unwanted conditions is highly dependent on the kind of condensation regime established and the consequent induced water mixing. Broadly speaking, three main regimes can be established in DCC (Petrovic de With et al., 2007). *Chugging* at low mass fluxes and low temperatures, inducing large mixing and large pressure spikes. *Bubbling* at intermediate mass fluxes and large temperatures, introducing little mixing. *Jetting* at large mass fluxes over a broad range of temperatures creating large mixing.

Due to the non-linearity of the problem, it is evident that the evaluation of the temperature distribution in the pool cannot be established by simple theoretical analyses, but computational models are deemed necessary. Recently great advances in CFD simulations of DCC have been achieved. Tanskanen (Tanskanen et al., 2014) has shown qualitatively good predictions of chugging and cyclic behavior established in the POOLEX facility (Puustinen et al., 2013), with two phase flow Eulerian-Eulerian approach. Later Pellegrini et al. (Pellegrini et al., 2015),

* Corresponding author.
E-mail addresses: marco@n.t.u-tokyo.ac.jp (M. Pellegrini), okamoto@n.t.u-tokyo.ac.jp (K. Okamoto), benjamin.blaisot@toulouse-inp.fr (B. Blaisot), nejdet.erkan@ukaea.uk (N. Erkan).

https://doi.org/10.1016/j.nucengdes.2024.113312
Received 28 March 2024; Received in revised form 10 May 2024; Accepted 10 May 2024
Available online 15 May 2024

expanded the model of Tanskanen including a model of the steam-water interface following the Rayleigh Taylor Instability theory and extended the qualitatively good predictions to other experiments similar to POOLEX (Povolny et al., 2017).

Both Tanskanen and Pellegrini's models were validated only qualitatively because the experimental evidence is composed fundamentally of video acquisitions. In other words, it is not clear whether the mixing induced by chugging is correctly reproduced by their CFD model. In addition, the computational demand requested by their two-phase flow approach does not allow their models to be realistically applied to a long scenario at plant scales (i.e. time and space).

A promising approach for large scale application is the Effective Momentum and Heat Source method (EMHS) proposed by Li and Kudinov (Li and Kudinov, 2010), where the only effect of condensation on momentum and internal energy is modeled, with the momentum term being the most complex to be quantified and where the majority of research has been done (Villanueva et al., 2015) (Marcos et al., 2019). In their model the authors express the momentum term as a relation between an amplitude and a frequency, following the synthetic jet theory (Smith and Swift, 2003). In their approach the amplitude represents the distance travelled by the steam-water interface back into the pipe after each bubble implosion, while the frequency is associated to the cycle of this phenomenon.

Such cyclic behavior has been documented in various experiments with relatively large pipe diameters such as POOLEX with diameter, D = 0.2 m (Laine et al., 2013), SIET facility D = 0.2 and 0.1 m (Pellegrini et al., 2016), and the TITech facility D = 0.027 m (Laine et al., 2013). However, such cyclic behavior does not seem to exist with smaller pipe diameter (i.e. few mm), while pool mixing is still present as reported in the UTokyo facility with D = 4 mm (Song et al., 2015). This evidence leads to the conclusion that mixing in the pool is not only induced by the water jet discharged from within the pipe, but the bubble implosion itself is the precursor of the water mixing.

In this paper the authors will present PIV results of a small-scale facility, previously employed by Song et al. (Song et al., 2015), to clarify the mechanism of mixing induced by the bubble implosion during DCC. The authors have found that the water flow induced by the bubble implosion contains a number of similarities with continuous jets (e.g. velocity spreading). This new piece of knowledge adds another important tile to the physics of DCC (chugging in particular) and the related sets of quantitative velocity data and implosion frequencies are considered fundamental for the validation of computer models, such as two-phase flow CFD and EMHS methods.

2. Experimental facility and methodology

The experimental facility employed is schematically presented in Fig. 1 a). The main test section is a 2D-like pool with two transparent windows for image acquisition. On the one side a transparent vertical slit is inbuilt to allow the creation of a laser sheet in the region of interest within the pool. The pool is equipped with several T-type thermocouples on three different posts on the x direction and different height as indicated in Fig. 1 b). The uncertainties associated with the thermocouples and their positions are less than 1.2 % and 2.5 %, respectively. The maximum uncertainty for the temperature measurement of the SP was about ± 2.9 %. The pipe inlet is located 15 cm from the bottom of the pool and has an internal diameter of 4.2 mm, while the external diameter measures 6.3 mm. Saturated steam is generated in the boiler connected to the pipe inlet. A gas heater is installed between the boiler and the injection point to guarantee that the steam is slightly superheated. The temperature is set by a temperature controller connected to the heater. The steam mass flow rate is estimated by the input power at the boiler considering the latent heat of vaporization at the operating pressure. There is no direct measurement of the steam flow rate.

The laser employed is a Viasho Power Emitting a green light (532 nm wavelength) with continuous output. Two cylindrical lenses are used to

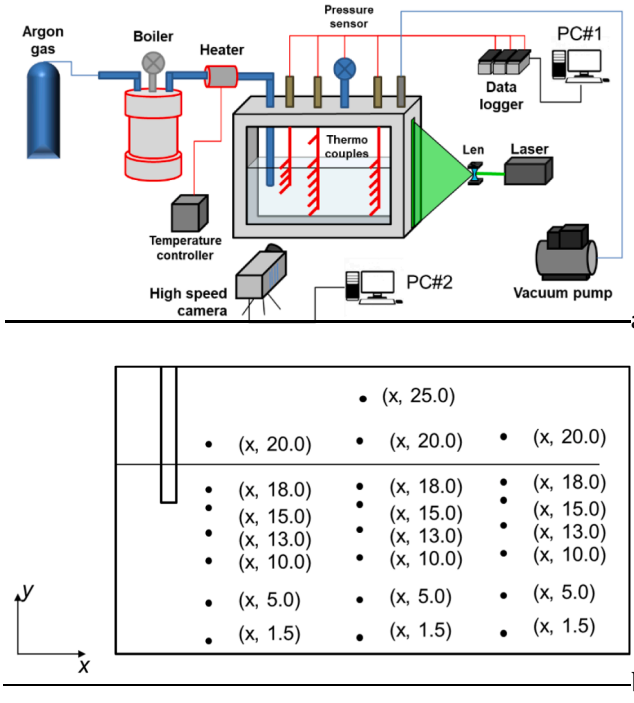

Fig. 1. A) schematic drawing of the whole facility at U-Tokyo and b) thermocouple location.

create the thinnest sheet right below the injection point and the widest in the vertical direction from the water surface to the pool bottom. The employed tracer for PIV is a HP2OSS resin fabricated by Mitsubishi Chemical Corporation with density 1.03 g/cm^3 covered with Rhodamine B. The size of the tracer is around 20 μm which guarantees a Stokes number of the order of magnitude of 10^{-5}. Rhodamine B is characterized by the absorption and emission spectrum presented in Fig. 2 a), red and light blue line respectively. A sharp-cut filter with the internal transmittance of nominal value around 560 nm is used to filter out all the laser reflections on the bubble, pipe and water surface, allowing the only emitted light to be detected by the high-speed camera.

The velocity measurement was performed by the PIV technique. The main categories of uncertainties for the velocity measurement were the calibration, image displacement, time interval and 3D effects. In terms of the calibration, the uncertainties from the image distance of reference points, physical distance of reference points, reference board position, parallel reference board, and image distortion by the lenses were 9.0 x 10^{-4}, 7.4 x 10^{-4}, 2.1 x 10^{-4}, 5.2 x 10^{-4}, and 2.1 x 10^{-4} mm/pixel, respectively. In terms of the image displacement, the uncertainty from the laser power fluctuation was 4.7 x 10^{-3} pixels. The uncertainties from the accuracy of the CCD and time interval were typically small and can be neglected. The uncertainty sources from the experiment were the particle trajectory and 3-D effects. The uncertainty from the particle trajectory can be estimated to be less than 0.01 % when the particle diameter is 50 μm and the relative density is 1.02 (Raffel et al., 1998). Although the uncertainty of the 3-D effect around the steam bubble interface was as large as 2.5 mm/s because of the complexity of DCC, the uncertainty of the flow far from the condensation area because of 3-D effects was estimate to be less than 0.1 mm/s. The random uncertainty because of cross-correlation error in the instantaneous velocity measurement is typically approximately 0.1 pixels (Westerweel, 1993).

The facility is equipped with a vacuum pump to allow experiments at lower saturation point. The vacuum pump is connected to a buffer tank of 60 L volume which guarantees a constant pressure during the experiment. However, the experiments presented hereafter are all conducted at atmospheric pressure.

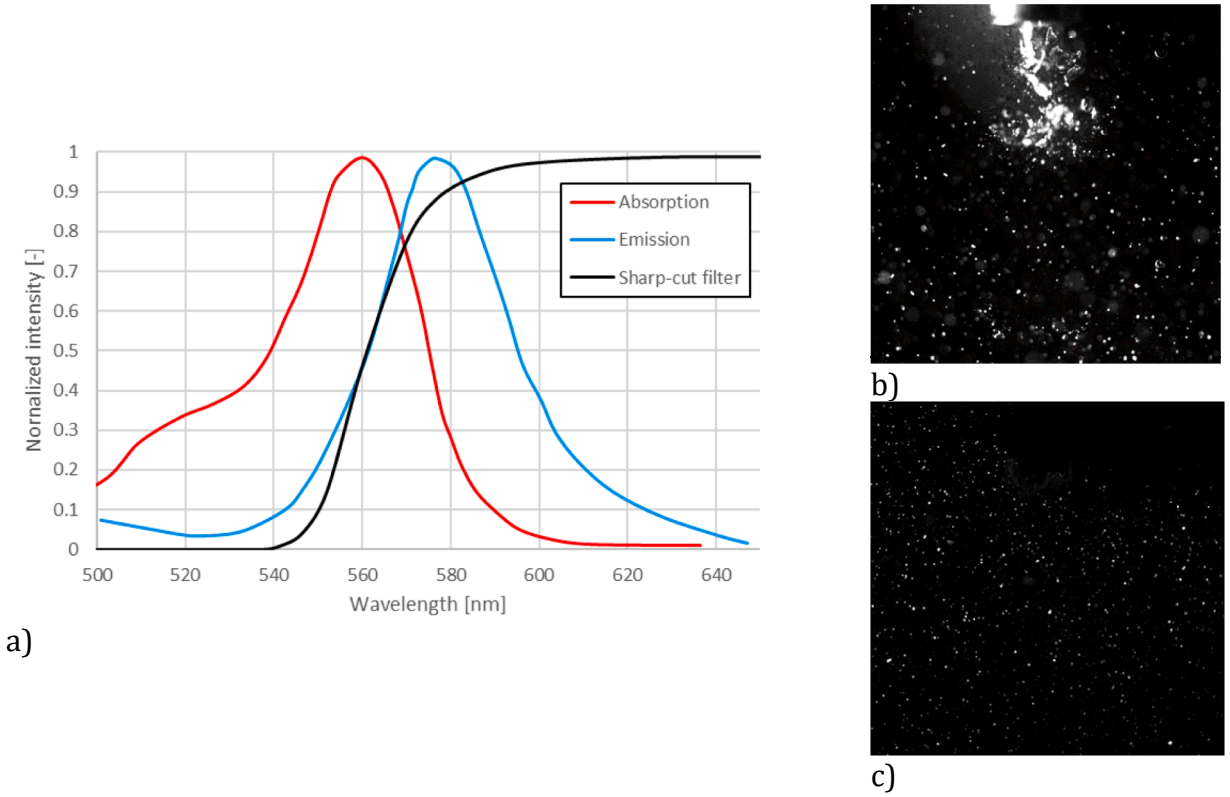

Fig. 2. A) absorption and emission characteristics of Rhodamine B, superposed with the sharp-cut filter characteristics.

2.1. Experimental procedure

Each experiment is carried out in the following way. First the pool is filled with water at room temperature until the water level reaches around 10 cm above the pipe outlet. The tracer is added to reach the desired concentration by visual observation. Subsequently the boiler is activated, steam generated and bypassed until saturated steam is obtained. Finally, steam is directed towards the pipe injection. The laser is activated, and power is adjusted until the tracers become clearly visible in the high-speed camera. The employed high-speed camera is a Fastcam SA-X Photron Limited and acquisition is performed at 10,000 fps for a total length of one second. As presented later with these settings around 50 implosions can be recorded and meaningful statistics can be obtained. High-speed camera acquisitions are taken every 10 degrees Celsius temperature interval referring to the thermocouple located in the highest position. During the experiment the steam condensation will go through chugging and bubbling stages until the pool surface temperature flattens out close to the water saturation point. At this point the experiment will be terminated. During chugging the temperature in the pool will be uniform, however in case of bubbling, stratification will be created.

A pioneering work on PIV performed on the same conditions, which is to say steam injected in a subcooled pool of water was presented in the past by Phillips et al (Philip et al., 1994). The authors had to develop a very innovative but convoluted technique due to camera limitations which allowed an acquisition rate of maximum 30 fps. Their approach hence involved two cameras and a pulse laser. In the present case, thanks to the very high acquisition rate of the camera (up to 100,000 fps) and the large power of the laser, the procedure is straightforward and the results available in larger quantities and conditions. Details of the conditions employed in one of the experiments are reported in the Table 1.

In literature a number of experiments have been performed to evaluate the condensation regimes based on the pool temperature and the steam mass flux. Works such as Youn et al (Youn et al., 2003), and Gregu et al. (Gregu et al., 2017) show a variety of condensation diagrams depending on the pool temperature and the mass flux where differences can be observed in the condensation maps. The main reason for the differences is that condensation depends also on the nozzle diameter, which is for the works above ranging from 15.9 to 19 mm and 27.0 mm respectively. As presented in Table 1, the nozzle employed in the experiment has an internal diameter of 4.2 mm, hence our experiments cannot be compared with the available diagrams of the two authors above. To the best of the authors' knowledge, experiments investigating condensation diagrams with a pipe diameter of around 4 mm do not exist in literature. From the work of Song et al. (Song et al., 2015) in the same facility it is clear that the investigated regimes belong to the internal chugging, meaning that the bubble is created downstream of the pipe outlet (not encapsulating) and the collapse occurs suddenly, condensing steam up to the steam inlet. As the pipe diameter of the facility is quite small, steam moving upstream the pipe is considered negligible.

Table 1
Details of the reported experiment.

Voltage	80.1	[V]
Current	5.86	[A]
Power	469.4	[W]
Latent Heat	2256.54	[J/g]
Mass Flow Rate	0.21	[g/s]
Mass Flow Rate Error	5%	[-]
Nozzle Internal Diameter	4.2	[mm]
Mass Flux	16.55	[g/m^2-s]

2.2. PIV analysis procedure

The PIV analysis is performed with the MATLAB package PIVlab ©. The velocity analysis is performed for the whole 10,000 frames.

Standard preprocessing is applied, and three interrogation windows are selected, respectively 128, 64 and 32. A check for cross correlation is allowed. The software allows for parallelization of the analysis which is active only in case the video has been saved in advance into each single frame. After the analysis, post-processing is completed filtering low contrast and bright objects. In general, correlation coefficients higher than 0.8 are found everywhere in the domain except close to the pipe outlet where the bubble grows and implodes. This occurs because during the bubble growth the area appears dark and occasionally reflections on the bubble surface of the light emitted by the particles is detected, which generates error in the code. This error is considered acceptable as the region of interest of this analysis is far from the pipe outlet, specifically in the jet spreading area. In the present work the challenges related to the variation of water refractive index with increasing temperature are not considered.

3. Results and discussions

The temperature readings obtained during the experiment are presented in Fig. 3. The thermocouples reading shows that the pool is well mixed until around 60 °C measured by the highest thermocouple in the water (i.e. 18 cm). This is created by mixing induced by chugging. Later on, in the experiment chugging chases and the bubbling regime does not create considerable mixing, thus temperature stratifies from around 2100 s.

3.1. Chugging analysis

Results of the PIV analysis is presented hereafter. Fig. 4 shows the results of four frames during a single bubble implosion at T_{water} equal 60 °C with T = 0.0 s representing the initiation of the implosion. The top row shows the raw image acquisition, the second one shows the measured vectors, the third shows the horizontal velocity (i.e. *u velocity*) and the fourth the vertical velocity (i.e. *v velocity*). From these frames it is possible to understand the mechanism of the mixing induced by the bubble implosion. Indeed, once the bubble collapses the surrounding water accelerates towards the singular point and a jet is generated in the direction opposite to the injecting pipe, which acts as a wall. The large horizontal velocity visible in the first two frames of the third row, is transferred as a vertical velocity in the last two frames of the fourth row (*v velocity*). From this figure we can notice that the area on the right side of the bubble appears darker because the bubble weakens the laser sheet. This might create inaccuracies in the velocity prediction in that location. As the focus of the paper is however on the velocity far from the bubble implosion's location, such inaccuracy does not invalidate the further discussion.

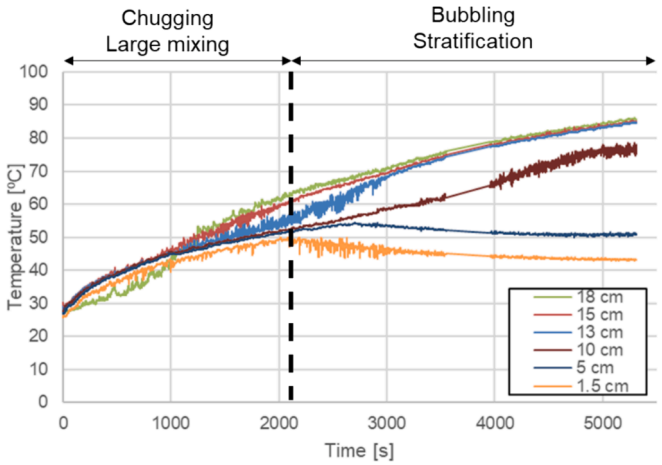

Fig. 3. Temperature history in the center post.

Fig. 5 a) and b) shows the maximum horizontal velocity in the domain over the recorded period for T_{pool} = 40 °C and 60 °C. with the objective to detect the frequency of the implosion. The horizontal velocity was chosen instead of the vertical velocity because it is representative of the time of the implosion while the vertical velocity could be affected by the previous implosion and mask out the correlation of each peak with each implosion. From this analysis it is straightforward to evaluate the period of the bubble implosion and its standard deviation to investigate the nature of the chugging phenomenon. The analysis of the period and its standard deviation are presented in Fig. 6 a) showing that no large difference and not a clear trend exists due to the water pool temperature regarding the frequency of the phenomenon. Hence, the period might be dependent only on the pipe size and steam flow rate. This can be explained as the vertical velocity is the result of the bubble implosion and no clear differences exist in the initial bubble size or the time of the implosion, which is around 2 ms, due to the temperature difference. As the mass flow rate is the same and the frequency is dependent on the size the bubble reaches at the time of the implosion, this means that the main mechanism leading to the implosion is independent of the subcooling. The small variance indicates that the phenomenon is clearly periodic during the chugging period. This finding is clearly different from what has been discussed in the work of Villanueva, Kudinov (Li and Kudinov, 2010) (Villanueva et al., 2015) but not in contradiction.

In their work the period was dependent on the temperature, however the evaluated period represented the time from two bubble implosions but including the time of the steam-water interface to being drawn within the pipe until a certain height. This phenomenon has been recorded only for large pipes while for small pipes the steam-water interface is always located close to the pipe outlet as in the present experiments.

Fig. 6 b) shows an increasing trend in the average maximum velocity in the horizontal and vertical directions. Despite what mentioned above that the frequency does not depend on the subcooling, the overall resulting water jet velocity might increase as the density of the water reduces with increasing temperature.

In the work by Yang et al. (Yang et al., 2019) with a pipe diameter equal to 9.525 mm the frequency is evaluated as the inverse of the condensation period. In their work as well, the frequency shows a clear dependency with the pool temperature and flow rate. While, as mentioned above in the present work such dependency is not clearly visible. This can be attributed to two main differences between the works. Yang et al. evaluate the bubbling period, while in this work the phenomenon investigated is chugging, whose physics is fundamentally different. In addition, Yang et al. performed experiments with an upwards jet, while in our case the jet direction is downwards. As Yang et al. mentioned, a downward injection might generate larger recirculation which maintains the heat transfer coefficient is always large around the bubble, generating a negligible difference in the condensation mechanism depending on the temperature.

3.1.1. Chugging jet analysis

The mean average velocity contours taken over 10,000 frames are presented in Fig. 7 for water temperature equal to 40 °C and 60 °C respectively. The mean vectors show a clear organized velocity profile which is induced by the only bubble implosion. It is important to confirm whether the induced water flow behaves as a jet to drive modeling in lumped parameter codes. In free jet analysis the jet is characterized by a self-similar behavior (Pope, 2000). This means that the normalized radial velocity profile is the same independently on the downstream location and the vertical velocity collapses on a single curve as proven in Fig. 8 for water temperature 40 °C and 60 °C. The current analysis has been performed for locations up to around six diameters. The figure shows clearly that the normalized velocity collapses on a single curve and that the flow decays exactly like a free-stream jet. Future analyses will investigate the normalized velocity profiles further

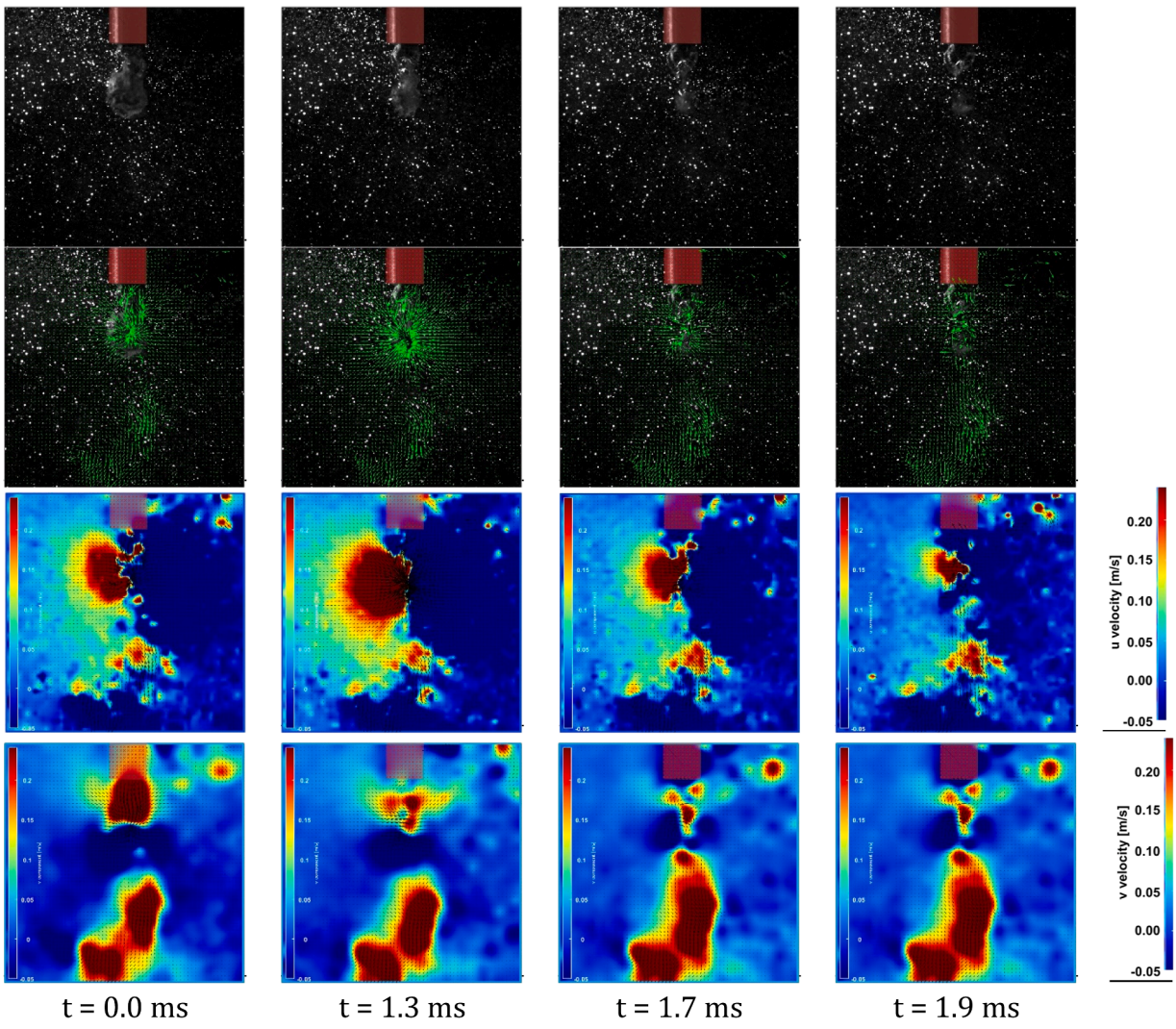

Fig. 4. example of PIV results during one bubble implosion at T_{pool} = 60 °C. Top row represents the image acquisition, second row the vectors, third row the u-velocity and bottom row the v-velocity. Videos of the velocity vectors and contour can be viewed at the following links: https://youtube.com/shorts/gN2GV1sWyNA?feature=share https://youtube.com/shorts/1o1d3k7hsYw?feature=share.

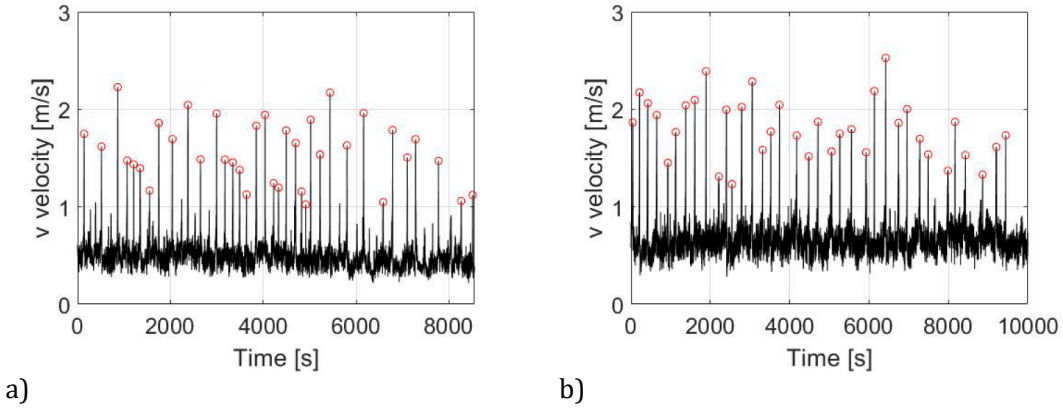

Fig. 5. Plot of the max u velocity in the domain a) 40 °C b) 60 °C.

downstream. Referring to Fig. 9 the self-similarity exists only from four diameters downstream the pipe outlet. This is because the region close to the pipe is characterized by the presence of the bubble, which is first growing and then imploding cyclically, hence characterized by low velocity. Fig. 9 presents the normalized vertical velocity, based on the maximum velocity on the centerline, in comparison with the free jet data by Todde et al. (Todde et al., 2009) at similar low Re number. The Reynolds number of the current experiment is evaluated considering characteristics velocity the maximum centerline velocity and characteristic diameter the pipe diameter. The properties of water are

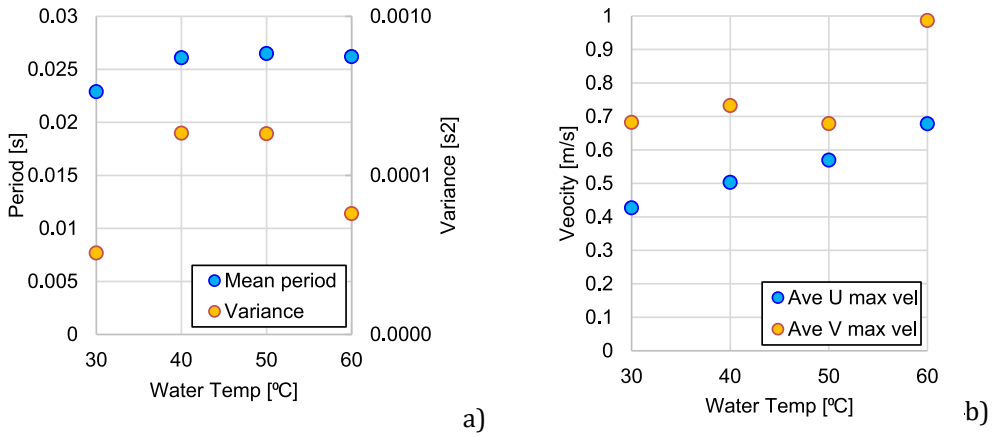

Fig. 6. A) analysis of period and its variance depending on the temperature, b) analysis of average u and v average velocities with increasing pool temperature.

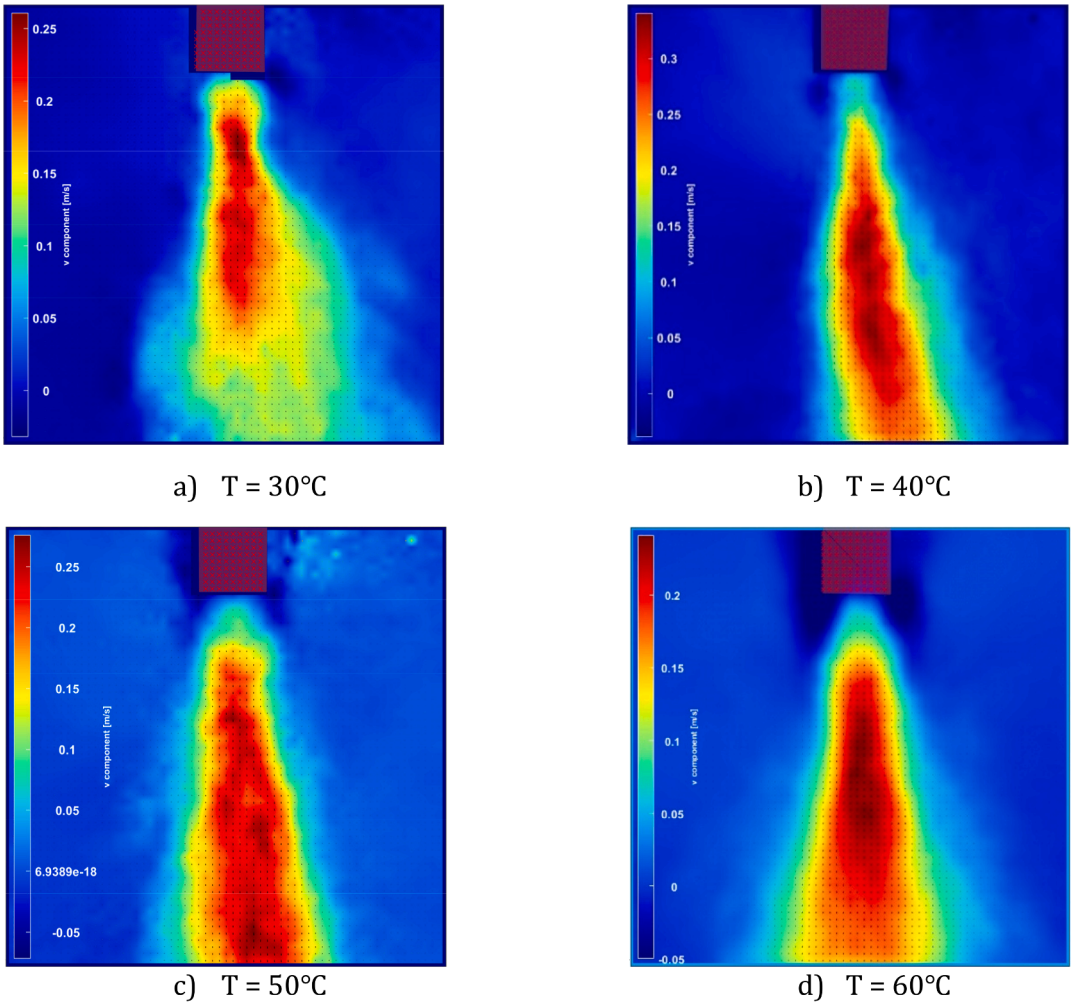

Fig. 7. Average v velocity contour a) T_{water} = 30 °C, b) T_{water} = 40 °C, b) T_{water} = 50 °C, b) T_{water} = 60 °C.

considered in the evaluation. The normalized jet vertical velocity in the work by Todde et al. is characterized by an entrance region, where the velocity is uniform and close to the maximum value. This region is followed by a spreading region where the velocity reduces.

The jet velocity measured in our experiments and superposed on the free jet case also shows an entrance region and a spreading region. In this particular case the transition between the two regions appears in the DCC-chugging experiments and the free jet occurs at the same normalized location downstream the pipe outlet, i.e. around five diameters. However, this result can be misleading, and it is believed that it occurs only by chance. Indeed, in the free jet case the entrance region represents the portion of the flow where the jet flow is undisturbed from the surrounding flow and proceeds with constant velocity. While in the DCC-chugging case the entrance region is the region which is occupied by the bubble, and which the measured velocity is low. Hence the two regions are physically not assimilable.

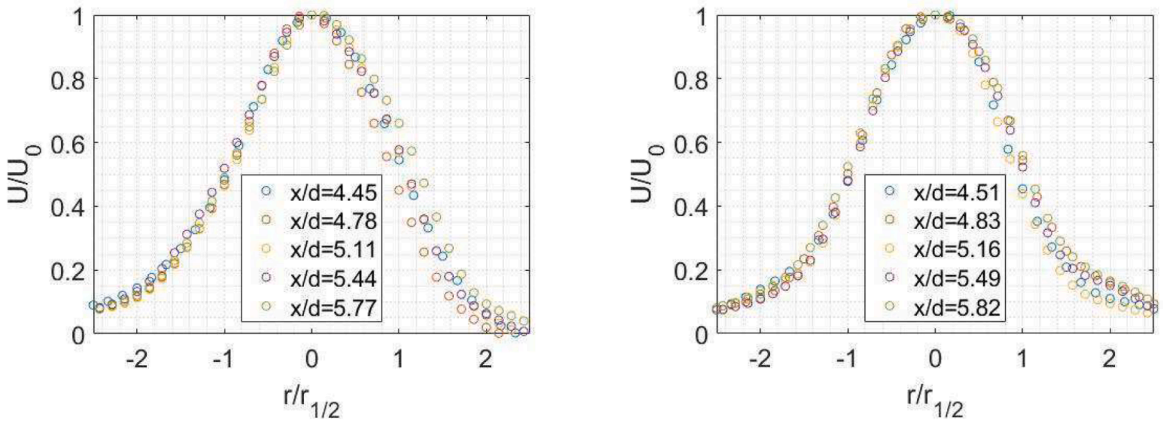

Fig. 8. Self-similar velocity profile at a) $T_{water} = 40$ °C, $T_{water} = 60$ °C.

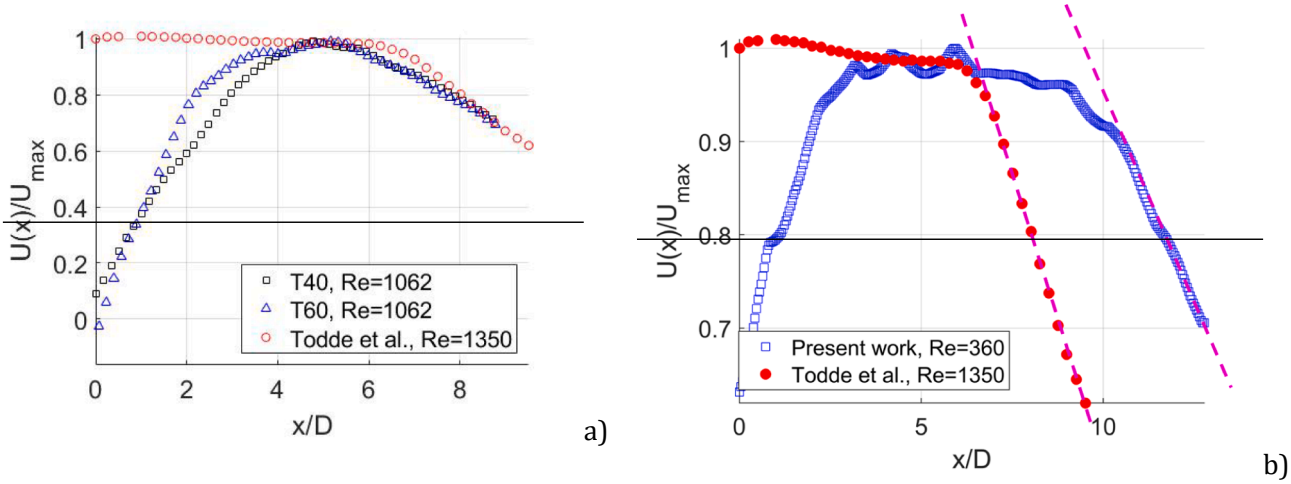

Fig. 9. Normalized centerline velocities comparison between jet induced by chugging and single phase at comparable Reynolds numbers.

It is nevertheless remarkable the comparison between the inclination of the velocity in the spreading region, which shows that the jet decays consistently way the case of Todde et al. (Todde et al., 2009). In both experiments the inclination of the slope is relatively similar. An additional experiment with a lower Reynolds number confirms that, while the entrance region is different, the decay downstream proceeds exactly like a single-phase water jet.

3.1.2. *Synthetic jet equivalent speed*

For the EMS modeling purposes it is useful to estimate the velocity as expressed from the synthetic jet theory

$$U_0 = \sqrt{2}fL$$

where f represents the frequency of the phenomenon and L is the characteristic length. From the period shown in Fig. 6a) and assuming the nozzle inner diameter as the characteristic length the resulting velocity follows very closely the measured value by the PIV technique as presented in Fig. 10.

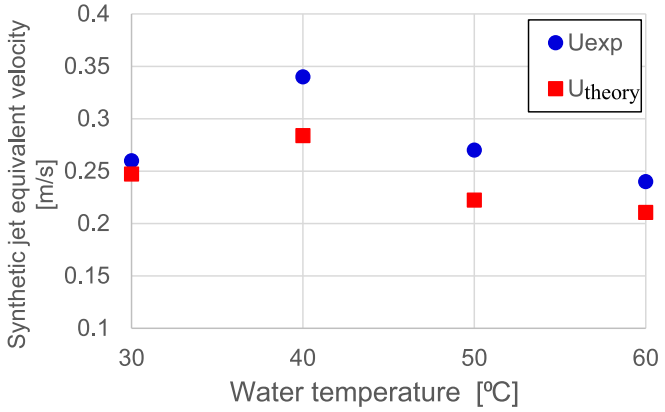

Fig. 10. Comparison between theoretical synthetic jet velocity and measured velocity.

4. Conclusions

In this work the PIV measurement for steam chugging implosion was performed with two main objectives. Firstly, to extract quantitative data for CFD validation and EMHS methods. Second, to understand more deeply the chugging phenomenon and the effect on the pool mixing. With the PIV measurement it was possible to extract the frequency of the phenomenon in more detail compared to simple visualization as done in the past (Song et al., 2015) and it was demonstrated that for this particular configuration, the frequency of the implosion phenomenon is not dependent on the pool temperature as hypothesized in past studies (Li and Kudinov, 2010) (Villanueva et al., 2015) (Marcos et al., 2019). This might be the result of the jet direction (i.e. downwards) and small nozzle diameter even though more research is necessary on the topic. It

was also demonstrated that the jet induced by the bubble implosion behaves effectively as a single-phase flow jet respecting the laws of self-similarity with an entry region whose length was not yet quantified and deferred to future studies. This is of particular importance in the modeling aspects of the EMHS methods. Additional work is necessary to demonstrate the mechanisms of the bubble implosion, which are still under discussion in the community (Ueno et al., 2015). For example, whether the implosion proceeds as a Rayleigh-Taylor Instability as hypothesized by (Pellegrini et al., 2015). Future work will challenge this aspect focusing on larger detail on the single bubble implosion including the exploration of the effect of larger pipe diameters and flow rates. Future research might target the case when steam does not condense abruptly where water entrainment might become the important variable to consider for modeling. This condition will be established when the water subcooling is reduced or when non-condensable gases are introduced in the steam flow.

CRediT authorship contribution statement

M. Pellegrini: Writing – review & editing, Writing – original draft, Visualization, Validation, Methodology, Investigation, Funding acquisition, Conceptualization. **K. Okamoto:** Funding acquisition. **B. Blaisot:** Methodology. **N. Erkan:** Validation.

Declaration of competing interest

The authors declare the following financial interests/personal relationships which may be considered as potential competing interests: Marco Pellegrini reports financial support was provided by Tokyo Electric Power Company Memorial Foundation If there are other authors, they declare that they have no known competing financial interests or personal relationships that could have appeared to influence the work reported in this paper.

Data availability

Data will be made available on request.

Appendix A. Supplementary data

Supplementary data to this article can be found online at https://doi.org/10.1016/j.nucengdes.2024.113312.

References

Abdulwahid, A.A., Situ, R., Brown, R.J., 2018. Underground Diesel Exhaust Wet Scrubbers: Current Status and Future Prospects. Energies 11, 3006.

Gregu, G., Takahashi, M., Pellegrini, M., Mereu, R., 2017. Experimental study on steam chugging phenomenon in a vertical sparger. Int. J. Multiphase Flow 88, 87–98.

R. T. Lahey, F. J. Moody, "*The thermal-hydraulics of a boiling water nuclear reactor*", Chapter 11, American Nuclear Society, La Grange Park, Illinois USA.

J. Laine, M. Puustinen, A. Räsänen, "PPOOLEX experiments on the dynamics of free water surface in the blowdown pipe", NKS-281, 2013.

Li, H., Kudinov, P., 2010. "Effective approaches to simulation of thermal stratification and mixing in a pressure suppression pool", CFD4NRS-3 Workshop. Bethesda, MD, USA.

I. G.-Marcos, P. Kudinov, W. Villanueva, R. Kapulla, S. Paranjape, D. Paladino, J. Laine, M. Puustinen, A. Räsänen, L. Pyy, E. Kotro, "Pool stratification and mixing induced by steam injection through spargers: CFD modelling of the PPOOLEX and PANDA experiments", Nuclear Engineering and Design, Vol. 347, 2019.

NEA/CSNI/R(2009)5, "*State-of-the-art report on nuclear aerosols*", Chapter 3.6, 2009.

Pellegrini, M., Araneo, L., Ninokata, H., Ricotti, M., Naitoh, M., Achilli, A., 2016. Suppression pool testing at the SIET laboratory: experimental investigation of critical phenomena expected in the Fukushima Daiichi suppression chamber. Journal of Nuclear Science and Technology 53 (5), 614–629. https://doi.org/10.1080/00223131.2015.1134359.

M. Pellegrini M. Naitoh C. Josey E. Baglietto Modeling of Rayleigh-Taylor instability for steam direct contact condensation The 16th International Topical Meeting on Nuclear Thermal Hydraulics (NURETH-16) 2015 Chicago, USA.

Petrovic de With, A., Calay, R.K., de With, G., 2007. Three-dimensional condensation regime diagram for direct contact condensation of steam injected into water. International Journal of Heat and Mass Transfer 50, 1762–1770.

Philip, O.G., Schmidl, W.D., Hasan, Y.A., 1994. Development of a high-speed particle image velocimetry technique using fluorescent tracers to study steam bubble collapse. NED 149, 375–385.

Pope, S.B., 2000. Turbulent Flows, Chapter 5 Free shear flows. Cambridge University Press.

Povolny, A., Kikura, H., Pellegrini, M., Naitoh, M., 2017. "improving accuracy of CFD modelling for direct contact condensation in a suppression pool", The 17th International Topical Meeting on Nuclear Thermal Hydraulics (NURETH-17). Xi'an, China.

M. Puustinen R. Kyrki-Rajamäki V. Tanskanen A. Räsänen H. Purhonen V. Riikonen J. Laine E. Hujala BWR suppression pool studies with POOLEX and PPOOLEX test facilities at LUT The 15th International Topical Meeting on Nuclear Thermal Hydraulics (NURETH-15) 2013 Pisa, Itay.

Raffel, M., Willert, C., Kompenhans, J., 1998. Particle Image Velocimetry: A Practical Guide. Springer-Verlag, Berlin.

Smith, B.L., Swift, G.W., 2003. A comparison between synthetic jets and continuous jets. Exp. Fluids 34, 467–472.

Song, D., Erkan, N., Jo, B., Okamoto, K., 2015. Relationship between thermal stratification and flow patterns in steam-quenching suppression pool. International Journal of Heat and Fluid Flow 56, 209–217.

Tanskanen, V., Jordan, A., Puustinen, M., Kyrki-Rajamäki, R., 2014. CFD simulation and pattern recognition analysis of the chugging condensation regime. Annals of Nuclear Energy 66.

Todde, V., Spazzini, P.G., Sandberg, M., 2009. Experimental analysis of low-Reynolds number free jets Evolution along the jet centerline and Reynolds number effects. Exp Fluids 47, 279–294.

Ueno, J., Ando, Y., Koiwa, T.S., Kaneko, T., 2015. Condensation and collapse of vapor bubble injected to subcooled pool. Eur. Phys. J. Special Topics 224, 415–424.

Villanueva, W., Li, H., Puustinen, M., Kudinov, P., 2015. Generalization of experimental data on amplitude and frequency of oscillations induced by steam injection into a subcooled pool. Nuclear Engineering and Design 295, 155–161.

Westerweel, J., 1993. Digital Particle Image Velocimetry: Theory and Application. Delft University Press, Delft, The Netherlands.

Yang, S.R., Seo, J., Hassan, Y.A., 2019. Thermal hydraulics characteristics of unstable bubbling of direct contact condensation of steam in subcooled water. Int. Journal of Heat and Mass Transfer 138.

Youn, D.H., Ko, K.B., Lee, Y.Y., Kim, M.H., 2003. The direct contact condensation of steam in a pool at low mass flux. J. Nucl. Sci. Technol. 40.